Available online at www.sciencedirect.com
ScienceDirect
Trans. Nonferrous Met. Soc. China 25(2015) 2388−2397
Transactions of Nonferrous Metals Society of China
www.tnmsc.cn

Adsorption mechanism of 2-mercaptobenzothiazole on chalcopyrite and sphalerite surfaces: *Ab initio* and spectroscopy studies

Fen JIAO, Wen-qing QIN, Rui-zeng LIU, Xing-jie WANG

School of Minerals Processing and Bioengineering, Central South University, Changsha 410083, China

Received 16 June 2014; accepted 12 May 2015

Abstract: Interaction mechanism of the collector, 2-mercaptobenzothiazole (MBT), with chalcopyrite and sphalerite surfaces were investigated by Fourier transform infrared (FTIR) and density functional theory. Results of FTIR showed that some characteristic peaks of MBT were observed on the chalcopyrite surface, including C═N, C═N—S and C—S stretching vibration peaks, and the adsorption product was CuMBT. But there were no characteristic peaks of MBT on the sphalerite surface. The thione molecular form of MBT was the most efficient and stable, N and exocyclic S were the more favourable reactive sites for nucleophilic attacked by metal atoms. Compared with ZnS (110), MBT is more readily adsorbed on $CuFeS_2$ (112). Attachment of MBT occurs due to strong bonding through exocyclic S p and s orbits with Cu d orbit on $CuFeS_2$ (112) and electron transfer from Cu atom to S atom. Under the vacuum condition, MBT in the form of thione molecular cannot be adsorbed on ZnS (110) spontaneously.

Key words: chalcopyrite; sphalerite; 2-mercaptobenzothiazole; adsorption mechanism; density functional theory

1 Introduction

With the mineral resources rapidly becoming depleted, fine-grained and complex, the flotation becomes more and more difficult. Unintentional (accidental) activation of minerals by contaminant metal ions is one source of mineral misplacements in separation by flotation reported by RASHCHI and FINCH [1]. Recently, much attention has been paid on searching for new chemical reagents which have a stronger affinity and better selectivity for certain metal ions [2−8], because the choice of collector type is crucial in the flotation performance of minerals.

2-mercaptobenzothiazole (MBT), was found to be alternatives to conventional xanthate collectors, and it has a lower dosage required to obtain high recoveries in sulfide-mineral flotation [9]. It has been suggested as a new collector in the flotation of metal sulfide ores, precious metal ores, gold-bearing pyrite, tarnished and secondary Cu, Pb and Zn minerals [2,10]. In our previous work [11], we found that in the presence of isopropyl ethylthionocarbamate, butyl xanthate, and ammonium dibutyl dithiophosphate, the separation between chalcopyrite and marmatite could not be achieved at neutral pH. MBT is as powerful as the other three collectors for the chalcopyrite, but it is a more selective collector against copper-activated marmatite at neutral pH and even better at alkaline pH. SZARGAN et al [12] investigated the adsorption of MBT on galena and pyrite surfaces by X-ray photo-electronic spectroscopy (XPS). They concluded that in 1×10^{-5} mol/L aqueous solution, MBT chemisorbed on the mineral surfaces via the thiolate group in monolayers. It was proposed that MBT adsorption on PbS occurred according to the mechanism that MBT−Pb formed on the PbS surface confirmed by FTIR investigations [3], and MBT bonded to Pb atom on the PbS surface through the exocyclic sulfur atom. Besides, MBT is used as the collectors in mineral processing. It is also used as effective corrosion inhibitors because MBT can form hydrophobic complexes with many metals such as Fe, Cu, Co and Ni [13−15]. Therefore, thorough studies on the electronic structure and reactivity between MBT and surfaces are necessary.

Many modeling studies have been carried out on the

Foundation item: Project (51274255) supported by the National Natural Science Foundation of China; Project (502042012) supported by the Postdoctoral Research Station of Central South University, China; Project supported by Co-Innovation Center for Clean and Efficient Utilization of Strategic Metal Mineral Resources, China

Corresponding author: Wen-qing QIN; Tel: +86-731-88830884; E-mail: qinwenqing369@126.com

DOI: 10.1016/S1003-6326(15)63854-7

collectors [16−18] and minerals [19−25]. STEELE et al [26] performed calculations of possible modes of interaction of Pb^{2+} ions with the (110) surface of sphalerite by using DFT to treat electron correlation. BLANCHARD et al [27] investigated the influence of incorporation of arsenic in FeS_2 pyrite, and they predicted that the formation of AsS dianion groups on FeS_2 surface is the most energetically favorable mechanism [28]. In order to probe the adsorption of Cu on pyrite (100), theoretical calculations were performed by OERTZEN et al [29] by using *ab initio* density functional theory, which supported the interpretation of the spectroscopy. In order to better understand the surface passivation in the leaching of chalcopyrite, OLIVEIRA et al [30,31] studied the reconstruction of (001), (100), (111), (112), (101) and (110) chalcopyrite surfaces by DFT calculations within the plane wave framework. Three different mechanisms were proposed: S^{2-} ions migrated to the surface tended to oxidize to form disulfides S_2^{2-}, while the superficial Fe^{3+} was concomitantly reduced to Fe^{2+}; metal atom moved downward to the surface and metallic-like bidimensional alloys formed underneath the surface, which were in good agreement with the results of XPS [32]. As stated previously, it was well established that DFT calculations were used in studying the electronic and molecular properties of collectors and minerals, and the adsorption mechanisms have been well recognized.

As MBT is more selective towards copper−zinc sulfide minerals than conventional collectors, to obtain further insights into the MBT−mineral surfaces interactions, the present communication presents the studies of the interactions of 2-mercaptobenzothiazole (MBT) with chalcopyrite and sphalerite surfaces by using FTIR and density-functional theory (DFT). The flotation process of sulfide minerals involves many factors that are beyond the scope of this study, such as pH, pulp potential [33−35], water, surface defects [19,37,38] and reconstruction [30,31,38]. Even a full description of solid−liquid interface is still a difficult task for the present quantum-chemical methods, hence it is important to start with a simple model for this theoretical investigation. Therefore, in this work, we only considered the adsorptions of MBT on perfect chalcopyrite (112) and sphalerite (110) surfaces.

All of the results aimed to contribute to the knowledge of the chemical reactivity of the chalcopyrite and sphalerite surfaces at a molecular level. Although the results calculated in this work show a good agreement with experimental observations, future investigation will have to be focused on the effects of different exposure atoms and surface reconstructions in order to better understand the adsorption mechanisms of reagents on mineral surface in flotation.

2 Experimental

2.1 Fourier transform infrared test

High-purity chalcopyrite, sphalerite and marmatite samples used in the test were obtained from Dachang concentrator, Guangxi, China. The chemical analysis of the chalcopyrite sample showed 35.90% Cu, 33.99% S and 29.17% Fe. The sphalerite sample contained 66.63% Zn, 32.13% S and 0.16% Fe. The samples were dry ground using a porcelain ball mill at a speed of 80 r/min. Then, the ground samples were dry screened and <37 μm sized fraction was used. The infrared spectra were recorded by NEXUS−470 spectrometer operating in the range of 4000−400 cm^{-1}. A mass of mineral sample (1 g) was mixed with 20 mL of reagent solution at pH 6.86 and then ground in an agate mortar for 30 min, filtrated, and rinsed twice or three times using the corresponding pH buffer solution. Subsequently, the sample was dried in a vacuum desiccator at 25 °C, and then used for FTIR reflection spectra measurement. The KBr pellet technique was adopted for recording the spectra.

2.2 Computational details

The quantum chemical calculations were performed using the Materials Studio 5.5 program CASTEP within the framework of nonlocal density functional theory using the generalized gradient approximation (GGA) of PERDEW et al [39]. The Perdew, Burke and Ernzerhof (PBE) functional models were carried out to study MBT adsorption on chalcopyrite and sphalerite surfaces [39]. Valence electron configurations in this work included Zn $3d^{10}4s^2$, S $3s^23p^4$, Cu $3d^{10}4s^1$, and Fe $3d^64s^2$. To model bulk properties using the super cell formalism, a suitable model system was constructed, and then repeated periodically. The size of the super cell must be sufficiently large to avoid spurious effects caused by interaction of the model system with its images.

Chalcopyrite crystallizes in tetragonal group with four formulas per unit cell; the space group is *I*-42*d*. The lattice parameters were determined by KNIGHT et al [40] to be $a=b=5.29$ Å and $c=10.4217$ Å. When the mineral cleavage plane was constructed, the vacuum thickness was fixed at 10 Å, and then the surface free energies were calculated under the corresponding atomic layer number. The convergence test results of surface free energy of $CuFeS_2$ (112) and (101) slices are shown in Fig. 1. The formula is shown as follows:

$$E_{\text{surf}} = \frac{1}{2}\lim_{M\to\infty}\frac{E_{\text{latt}} - E_{\text{slice}}}{A_{\text{hkl}}} \quad (1)$$

where E_{latt} is the energy of body model with the same atomic number; E_{slice} is the energy of crystal surface model; A_{hkl} is the crystal surface area; 1/2 is the two

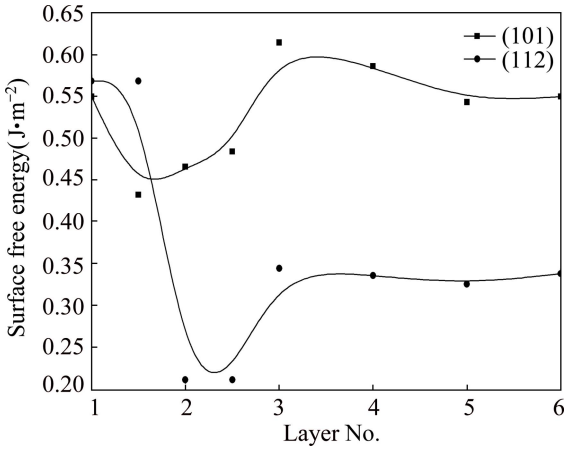


Fig. 1 Convergence test results of surface free energy of $CuFeS_2$ (112) and (101) slices

surfaces of the section.

It is shown from Fig. 1 that, when the layer number is small, the fluctuations of the two surface free energies are serious. The surface free energies tend to be stable when the layer number is larger than 3. The stabilizing value is the surface free energy. The lower the surface free energy is, the more stable the surface is. As shown in Fig. 1, the surface free energies of chalcopyrite (112) surface and (101) surface are 0.3359 and 0.5317 J/m^2, respectively. Thus, chalcopyrite (112) surface is more stable, which indicates that chalcopyrite can cleavage more easily in parallel with the (112) surface. So, (112) surface was chosen for further discussion.

The chalcopyrite (112) surface was simulated using a slab model considering a super cell (2×2×1) with two unit cells along directions *a* and *b* and 8 atomic layers in direction *c* with the top 4 atomic layers free to relax. To avoid the interaction between the slabs, a vacuum thickness of 10 Å was applied along direction *c*. The kinetic energy cutoff of 245.0 eV (Table 1) for the plane wave basis was used throughout the study, and *k*-points of 5×5×2 grid for all structure calculation. The energy tolerance, force tolerance, and displacement tolerance were 5.0×10^{-4} eV/atom, 0.01 eV/Å and 0.005 Å, respectively. The calculated lattice parameters were $a=b=5.2867$ Å, and $c=10.452$ Å.

The cell parameters of sphalerite are $a=b=c=5.41$ Å, and $\alpha=\beta=\gamma=90°$ [41]. The perfect ZnS (110) surface was modeled using 2×2×1 super cell with 9 atomic-layer slabs of ZnS and a vacuum thickness of 12 Å. The kinetic energy cutoff of 370.0 eV (Table 1) for the plane wave basis was used throughout the study, and k-points of 3×3×3 grid for all structure calculation, which were sufficient after convergence tests. The energy tolerance, force tolerance, and displacement tolerance were 5.0×10^{-6} eV/atom, 0.01 eV/Å and 0.0005 Å, respectively. The calculated lattice parameters were $a=b=c=5.37$ Å.

Table 1 Results of cut-off energy as function of GGA-PBE

Mineral (*k*-point)	Cut-off energy/eV	Cell constant/Å	Energy/eV
Chalcopyrite (5×5×2)	210	$a=b=5.2739$, $c=10.3811$	−11067.49
	245	$a=b=5.2698$, $c=10.3382$	−11076.97
	280	$a=b=5.1441$, $c=10.1257$	−11075.47
	300	$a=b=5.1247$, $c=10.0936$	−11076.48
	330	$a=b=5.1157$, $c=10.0581$	−11069.89
Sphalerite (3×3×3)	330	5.4521	−7957.67
	350	5.4527	−7957.70
	370	5.4447	−7957.86
	390	5.4411	−7957.79
	430	5.4390	−7957.77

The quantum chemical parameters of highest occupied molecular orbital energy (E_{HOMO}) and lowest unoccupied molecular orbital energy (E_{LUMO}) were obtained using the density functional theory and B3LYP/6−31G method in Gaussian 03.

3 Results and discussion

3.1 Infrared spectra

Infrared spectra were recorded for MBT, chalcopyrite, sphalerite, and the products of interaction between the mineral and MBT at pH 6.86. The FTIR spectrum of MBT is portrayed in Fig. 2. The bands at 1587.128 and 1492.633 cm^{-1} are the vibration adsorption peaks of C═C on aromatic ring. The C═N adsorption peak at 1690−1630 cm^{-1} originally occurs at 1500−1400 cm^{-1} due to the influence of surrounding environment. Because of the effect of ligand (S), the ring stretching vibration zone of C═N—S appears at 1400 and

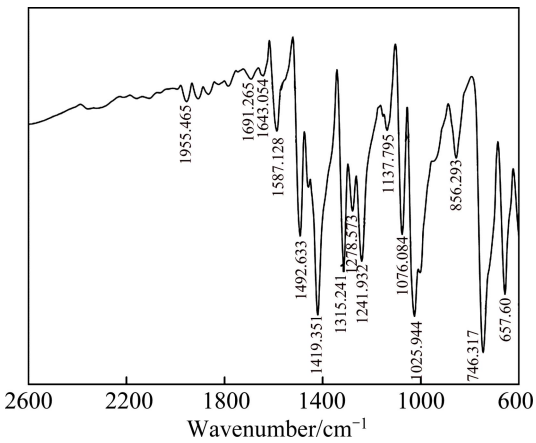


Fig. 2 FTIR spectrum for MBT

1430 cm^{-1}. Therefore, 1419.351, 1241.932, and 1025.944 cm^{-1} are C═N—S characteristic adsorption peaks, C—N on benzene ring stretching vibration band, and C—S stretching vibration peak, respectively. The band at 746.317 cm^{-1} is due to the four contiguous H atoms on benzene ring outward rocking vibration. In addition, the strong band at 657.60 cm^{-1} is attributed to the vibration of C—S.

The FTIR spectra of chalcopyrite and sphalerite before and after the interaction with MBT are depicted, respectively, in Figs. 3 and 4, respectively. The infrared spectra only show the 1800−900 cm^{-1} region, since this area includes most of the adsorption bands attributable to the MBT. In Fig. 3, after interaction with MBT, it is noteworthy that the bands at 1497.795, 1355.712, 1267.003, 1078.342, 1025.873, 875.104 and 642.18 cm^{-1} are present on chalcopyrite surface due to chemical interaction. These bands belong to stretching vibration peaks of C═N, C═N—S and C—S. Similar band at 1355.712 cm^{-1} has been reported by HOPE et al [42], which is due to the formation of CuMBT.

In Fig. 4, there is no significant change after interaction with MBT. It is found that there is a small migration of the peak at 1101.54 cm^{-1}, and the displacement value is 1.948 cm^{-1}. The results indicate that MBT adsorbs on sphalerite surface physically.

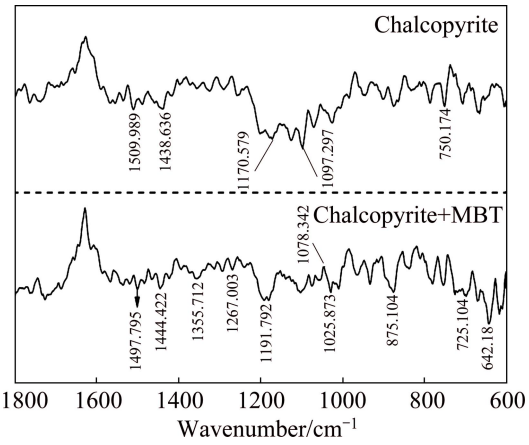


Fig. 3 FTIR spectra of chalcopyrite in absence and presence of MBT

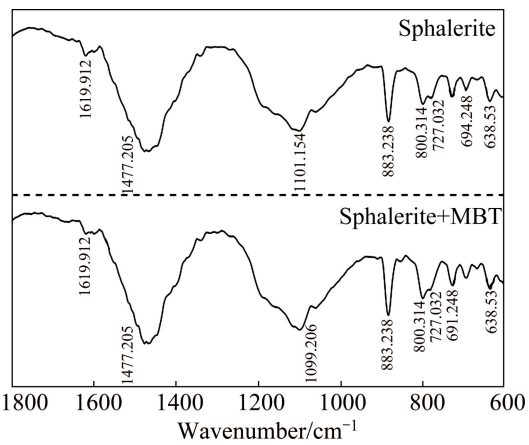


Fig. 4 FTIR spectra of sphalerite in absence and presence of MBT

3.2 Ab initio calculations

3.2.1 Stable form for MBT

In organic chemistry, MBT exists as thione and thiol tautomers. Therefore, there are four tautomers including ions and molecule shown in Fig. 5. FLEMMIG et al [43] investigated the electron, chemical bonding states and the adsorption on pyrite surface, and they concluded that the energies of thione molecule and ion were −879.502 and −873.034 eV, respectively. In addition, the energies of thiol molecule and ion were −875.735 and −868.891 eV, respectively. A smaller energy implies higher stability index. Therefore, MBT is more stable when it exists as thione. From the FTIR of MBT, it can be seen that there is no band of S—H in thiol near 2500 cm^{-1}, so, in this work, the thione tautomer is more stable than the thiol tautomer. To obtain further insights into the stable form of MBT, the ground-state geometries were fully optimized using the density functional theory and B3LYP/6−31G method in Gaussian 03. After optimization, the energies of thione molecule, thione ion, thiol molecule and ion are −1124.39, −1123.83, −1120.86 and −1120.36 eV, respectively, which indicates that thione molecular is the most stable form.

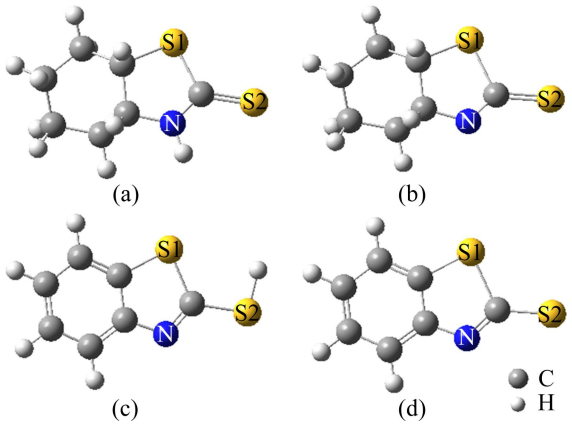


Fig. 5 Thione and thiol tautomers of MBT: (a) Thione molecule; (b) Thione ion; (c) Thiol molecule; (d) Thiol ion

The frontier orbitals of highest occupied molecular orbital energy (E_{HOMO}) and lowest unoccupied molecular orbital energy (E_{LUMO}) are related to the activity of a molecular. The formation of a transition state is due to an interaction between the frontier orbitals (HOMO and LUMO) of reactants according to the frontier molecular orbital theory [44]. It is well established that the higher HOMO energy value or less negative HOMO reflects that the molecule more easily releases the electrons to the unoccupied orbitals of the metal and stronger

chemisorbed band efficiency, thus the molecule has the strongest interaction with metal and the best collector ability [9].

So, the HOMO orbitals were taken into account here because the MBT and its tautomers react as electron-donor species in flotation. The HOMO maps are shown in Fig. 6. It can be seen that for the thione molecule and ion, HOMO orbitals lie mainly on the S2, S1 and N atoms; while for the thiol molecule and ion, whose HOMO orbitals are localized on the phenyl ring besides S2, S1 and N atoms. The order of HOMO energies in Table 1, from big to small, is thione molecule, thione ion, thiol molecule, thiol ion, which suggests that MBT in the form of thione molecule has the strongest interaction with metals on mineral surfaces.

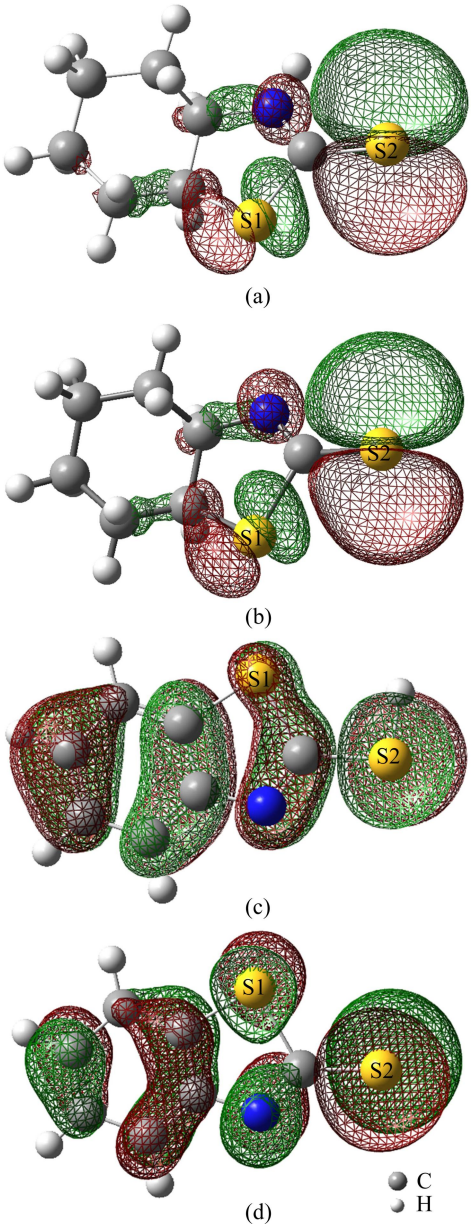


Fig. 6 HOMO for different forms of MBT tautomers: (a) Thione molecule; (b) Thione ion; (c) Thiol molecule; (d) Thiol ion

Mulliken population analysis, which is mostly used for the calculation of the charge distribution in a molecule, is another parameter for explaining the nucleophilic phenomena and in turn reflects the chelating ability. The atomic charge values are listed in Table 2 by Mulliken analysis. For the four species tested, it is observed that the S2 and N of the thione molecule present negative charges. The S1 atoms present positive charges and are poor donor atoms, which is attributed to the delocalization by resonance with the aromatic ring. A good agreement was found by WOODS et al [10]. Therefore, N and S2 on thione molecule are the more favourable reactive sites for metal atom.

Table 2 Results of calculated HOMO, LUMO energies and Mulliken charge of MBT species

Species	E_{HOMO}/eV	E_{LUMO}/eV	Mulliken charge/e		
			S1	S2	N
Thione molecule	−0.088	−0.071	0.570	−0.290	−0.237
Thione ion	−0.101	−0.084	0.132	−0.120	0.031
Thiol molecule	−0.112	−0.045	−0.489	−0.200	0.251
Thiol ion	−0.247	−0.040	−0.818	−0.506	0.194

In comparison, it can be obtained that the most stable status with the highest efficiency of MBT as a collector is in the form of thione molecule. As a result, the thione molecular was chosen for detailed investigation.

3.2.2 Adsorption of MBT on $CuFeS_2$ (112)

The interactions of the thione molecule with chalcopyrite and sphalerite surface were investigated aiming to understand the selectivity of MBT for the two minerals, which can provide some information for the separation of copper−zinc sulfide ore by flotation. In our approach, different adsorption sites of Cu and Fe for chalcopyrite (112) and Zn (*A*), (*B*) were considered. Figure 7 shows the optimized structures of chalcopyrite (112). The optimized Cu—S bond length was calculated to be 2.313 Å, which is in good agreement with the value of 2.300 Å obtained by SIESTA program [45]. The adsorption energy can be calculated by

$$\Delta E_{ads} = E_{MBT+surface} - E_{surface} - E_{MBT} \quad (2)$$

where E_{ads} is the adsorption energy; $E_{MBT+surface}$ is the final energy of the surface with MBT adsorbed on it, and $E_{surface}$ and E_{MBT} correspond to the final energies of the surface and MBT, respectively. A negative ΔE_{ads} means that the adsorption can occur spontaneously. The lower the ΔE_{ads} is, the more stable the formed complex is, and the larger the collecting capacity of the collector is [46].

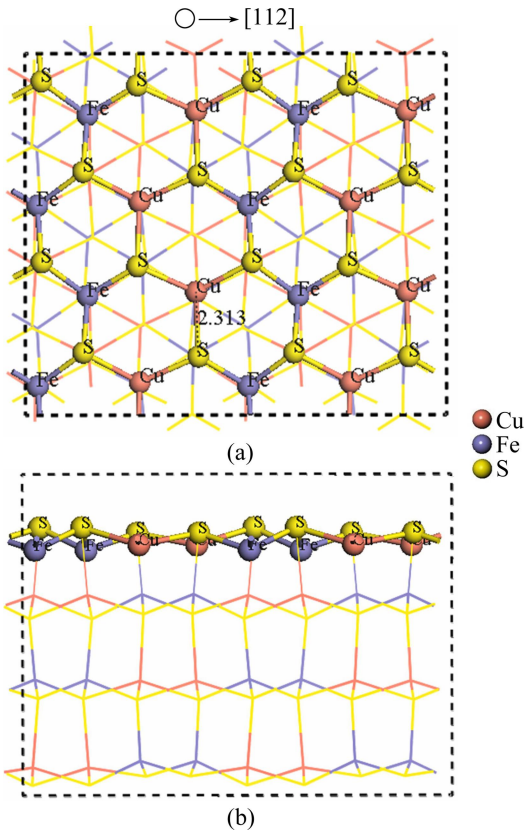


Fig. 7 Top (a) and side (b) views of $CuFeS_2$ (112) surface

The adsorption energies of all calculated adsorption sites are summarized in Table 3. For the (MBT−Cu) adsorption mode, the adsorption energy was calculated by Eq. (2) to be −185.1786 J/mol, which is smaller compared with the adsorption energy for the (MBT−Fe) mode. We believe that Cu atom is the more favorable adsorption site for MBT compared with Fe atom energetically. Cu is a soft Lewis acid explaining the preference of the sulfur ion to the copper adsorption sites. The optimized configuration of MBT in the form of thione molecular adsorption on Cu site is shown in Fig. 8. The bond length of S2—Cu is 2.204 Å, which is smaller than that of free S—Cu (3.01 Å). It is important to emphasize that, a strong chemi-adsorption occurs between MBT and Cu atom on $CuFeS_2$ (112).

The PDOSs projected over the Cu atom before and after adsorption are shown in Fig. 9, which indicates the peak at −4.4 eV of 3d orbital disappears and shifts to the conduction band after adsorption, suggesting that the Cu 3d orbital loses electrons and participates in the interaction with MBT. As can be seen from Fig. 10 that, the peak at −1.96 eV of 3p orbital of S2 on MBT

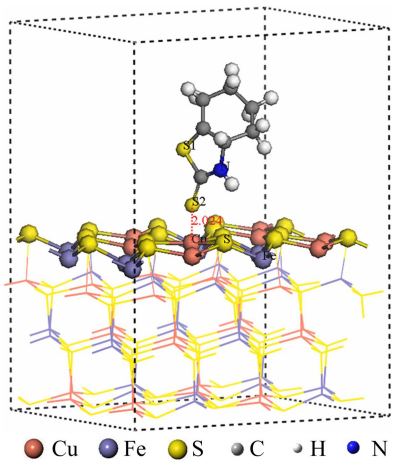


Fig. 8 Optimized configurations of MBT adsorption on Cu site on $CuFeS_2$ (112) surface

Table 3 Adsorption energies of MBT on mineral surfaces

Surface	Adsorption site	$E_{surface}$/eV	E_{MBT}/eV	$E_{MBT+surface}$/eV	E_{ads}/(J·mol^{-1})
$CuFeS_2$ (112)	Cu	−22136.8529	−2070.70	−24209.4758	−185.1786
	Fe	−22136.8529	−2070.70	−24206.8638	66.3617
ZnS (110)	Zn(*A*)	−71615.4786	−2070.70	−73679.4175	651.1061
	Zn(*B*)	−71615.4786	−2070.70	−73675.9068	989.1924

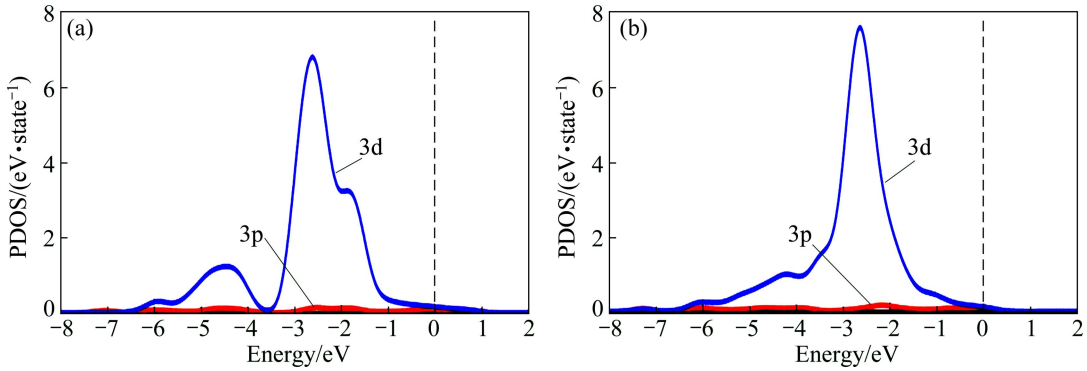


Fig. 9 PDOS of free (a) and adsorbed (b) Cu on $CuFeS_2$ (112) surface

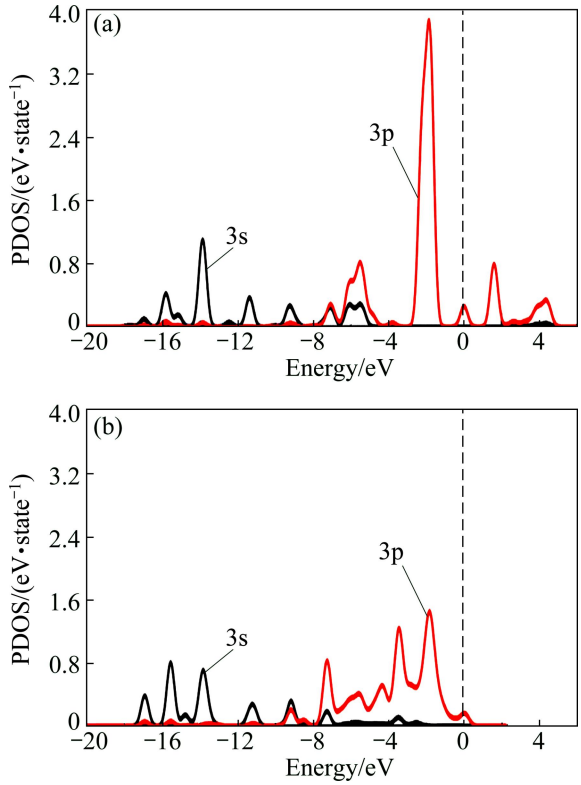


Fig. 10 PDOS of free (a) and adsorbed (b) S2 on MBT molecule

molecule becomes depleted and a portion of the 3p orbital moves evidently to the valence band after adsorption, which implies that the 3p orbital of S2 receives electrons. The whole movement of 3s orbital to the valence band occurs as shown in Fig. 10(b). It is proved that the 3s and 3p orbits of S2 of MBT participate in the reaction with Cu atom.

Further insights into the nature of S2 on MBT surface bonding with Cu on $CuFeS_2$ (112) surface can be obtained through the Milliken population analysis. Table 4 presents the Mulliken populations of Cu on $CuFeS_2$ (112) surface and S2 of MBT before and after adsorption. It can be seen that the population of d for Cu atom decreases, while the population of p for S2 atom increases simultanously. A good fit is obtained by the PDOS analysis.

The electron density difference between S2 on MBT molecule and Cu on chalcopyrite (112) surface is shown in Fig. 11. The panel is cut through the center of Cu and S2 atoms, herein, blue and red contours correspond to the depletion of electron density and increased electron density, respectively. The regions near Cu atom are blue, which implies a depletion of electron density; the regions around S2 atom are red, indicating an increase of electron density, which are in a good agreement with the findings of PDOS and Mulliken population analysis.

3.2.3 Adsorption of MBT on ZnS (110)

Figure 12 shows the optimized structures of

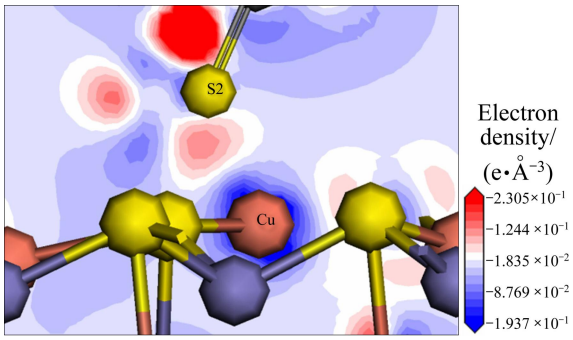


Fig. 11 Electron density difference of S2 and Cu

Table 4 Mulliken of Cu on $CuFeS_2$ (112) surface and S2 of MBT before and after adsorption

Atom	Adsorption state	Population/e				Mulliken charge/e
		s	p	d	Total	
Cu	Before adsorption	0.59	0.41	9.72	10.72	0.28
	After adsorption	0.59	0.40	9.66	10.65	0.35
S2	Before adsorption	1.92	4.24	0.00	6.16	−0.16
	After adsorption	1.91	4.33	0.00	6.24	−0.24

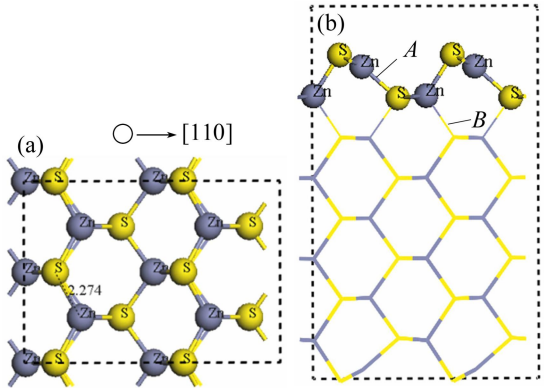


Fig. 12 Top (a) and side (b) views of ZnS (110) surface

sphalerite (110). Zn—S bond length is estimated to be 2.274 Å, which matches perfectly with the mean value of 2.29 Å [26]. In our test, two different adsorption sites of Zn atom have been considered. Based on the (2×2×1) super cell shown in Fig. 12, sites *A* and *B* of Zn over the superficial surface were tested. The adsorption energies calculated for the (MBT−Zn(*A*)) mode and (MBT−Zn(*B*)) modes are 651.1061 and 989.1924 J/mol (Table 3), respectively. It is noteworthy that, under vacuum condition, the MBT in the form of thione molecule cannot adsorb on the perfect ZnS (110) surface spontaneously.

The optimized configuration of MBT in the form of thione molecular adsorption on Zn (*A*) site is shown in Fig. 13. The bond length of S2−Zn is 2.439 Å, which is larger than that of S−Zn (2.430 Å) and there is no interaction between MBT and Zn (110) surface. The

calculated results are in good agreement with spectroscopy studies shown in Fig. 4.

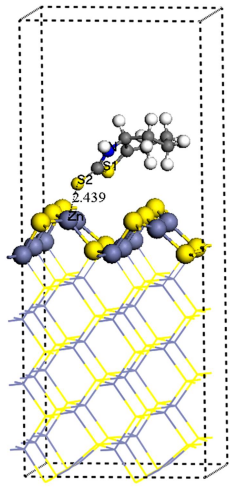


Fig. 13 Optimized configuration of MBT adsorption on Zn(*A*) site on ZnS(110) surface

Milliken population analysis was conducted and the results are shown in Table 5 to obtain further insights into the adsorption mechanism of MBT−ZnS(110) surface. It indicates that after adsorption there is no change for the atomic charges.

The previously study [16] indicated that the selectivity of the collectors was related to their molecular structure. The recovery of chalcopyrite was more than 96.23% in the presence of MBT (1.0×10^{-5} mol/L) and the marmatite recovery after activation ($c(CuSO_4)$= 1.0×10^{-4} mol/L) was 61.22%, which was lower than that of chalcopyrite. These ratios show the difference in the selectivity by MBT. Mechanisms are proposed in this study based on FTIR and computational analysis: A chemi-adsorption occurs for MBT and hydrophobic compound CuMBT forms on chalcopyrite surface, so the floatability is improved; nevertheless, MBT cannot adsorb on sphalerite surface spontaneously.

Table 5 Mulliken of Cu on $CuFeS_2$ (112) surface before and after MBT adsorption

Atom	Adsorption state	Population/e				Mulliken charge/e
		s	p	d	Total	
Zn	Before adsorption	0.83	0.84	9.98	11.65	0.35
	After adsorption	0.82	0.86	9.98	11.66	0.34
S2	Before adsorption	1.92	4.24	0.00	6.16	−0.16
	After adsorption	1.90	4.26	0.00	6.16	−0.16

4 Conclusions

1) The chemical parameters such as the frontier orbital energies and atomic charges, which can indicate the reactive behavior of MBT tautomers, were theoretically calculated and the adsorption mechanisms of MBT on chalcopyrite and sphalerite surfaces were determined by FTIR and DFT.

2) After conditioning with MBT, there were many characteristic peaks of MBT observed on chalcopyrite surface, which indicated a chemi-adsorption occurring; while a small migration of the peak at 1101.54 cm^{-1} appeared on sphalerite surface.

3) The thione molecular form of MBT was the most efficient and stable, and N and S2 on thione molecular were the more favourable reactive sites for nucleophilic attack by metal atoms.

4) The results of calculations indicated that Cu atom was the more favorable adsorption site for MBT compared with Fe atom energetically, and the adsorption energy was −185.1786 J/mol. Cu 3d orbital lost electrons and participated in the interaction with MBT, and the 3s orbital and 3p orbital of S2 of MBT received electrons. Under vacuum condition, the MBT in the form of thione molecular could not adsorb on the perfect ZnS (110) surface spontaneously.

5) Compared with our previous study, it was concluded that MBT was a more powerful collector for chalcopyrite than for sphalerite.

References

[1] RASHCHI F, FINCH J A. Deactivation of Pb-contaminated sphalerite by polyphosphate [J]. Colloids Surf A, 2006, 276: 87−94.

[2] YEKELER M, YEKELER H. A density functional study on the efficiencies of 2-mercaptobenzoxazole and its derivatives as chelating agents in flotation processes [J]. Colloids Surf A, 2006, 286: 121−125.

[3] CONTINI G, CICCIOLI A, COZZA C, BARBARO M, MARABINI A M. Infrared study of 2-mercaptobenzothiazole and two of its derivatives adsorbed on PbS [J]. Int J Miner Process, 1997, 51: 283−291.

[4] MAIER G S, DOBI Š B. 2-mercaptobenzothiazole and derivatives in the flotation of galena, chalcocite and sphalerite: A study of flotation, adsorption and microcalorimetry [J]. Miner Eng, 1997, 10: 1375−1393.

[5] FLEMMIG B, MAYER D, HALLMEIER K H, REINHOLD J, SZARGAN R. Characterization of the mercaptobenzothiazole bonding on cadmiumsulfide by MO interpretation of N K XANES results [J]. Chem Phys, 2002, 277: 117−123.

[6] COZZA C, DI CASTRO V, POLZONETTI G, MARABINI A M. An X-ray photoelectron spectroscopy (XPS) study of the interaction of mercapto-benzo-thiazole with cerussite [J]. Int J Miner Process, 1992, 34: 23−32.

[7] NATARAJAN R, NIRDOSH I. New collectors for sphalerite flotation [J]. Int J Miner Process, 2006, 79: 141−148.

[8] SHEN W Z, FORNASIERO D, RALSTON J. Effect of collectors, conditioning pH and gases in the separation of sphalerite from pyrite [J]. Miner Eng, 1998, 11: 145−158.

[9] MARABINI A M, BARBARO M, ALESSE V. New reagents in sulphide mineral flotation [J]. Int J Miner Process, 1991, 33: 291−306.

[10] WOODS R, HOPE G A, WATLING K. A SERS spectroelectrochemical investigation of the interaction of 2-mercaptobenzothiazole with copper, silver and gold surfaces [J]. J Appl Electrochem, 2000, 30: 1209−1222.

[11] QIN Wen-qing, JIAO Fen, SUN Wei, HE Ming-fei, HUANG Hong-jun. Selective flotation of chalcopyrite and marmatite by MBT and electrochemical analysis [J]. Ind Eng Chem Res, 2012, 51: 11538−11546.

[12] SZARGAN R, SCHAUFUß A, ROßACH P. XPS investigation of chemical states in monolayers: Recent progress in adsorbate redox chemistry on sulphides [J]. J Electron Spectrosc Relat Phenom, 1999, 100: 357−377.

[13] FENG Yuan-yuan, CHEN Shen-hao, ZHANG Hong-lin, LI Ping, WU Ling, GUO Wen-juan. Characterization of iron surface modified by 2-mercaptobenzothiazole self-assembled monolayers [J]. Appl Surf Sci, 2006, 253: 2812−2819.

[14] WU F L, HUSSEIN WALEED M, ROSS BENJAMIN P, MCGEARY ROSS R. 2-Mercaptobenzothiazole and its derivatives: Syntheses, reactions and applications [J]. Curr Org Chem, 2012, 16: 1555−1580.

[15] CONTINI G, DI CASTRO V, STRANGES S, RICHTER R, ALAGIA M. Gas-phase photoemission study of 2-mercaptobenzothiazole [J]. J Phys Chem A, 2002, 106: 2833−2837.

[16] GECE G. The use of quantum chemical methods in corrosion inhibitor studies [J]. Corros Sci, 2008, 50: 2981−2992.

[17] LIU Guang-yi, ZHONG Hong, XIA Liu-yin, WANG Shuai, DAI Ta-gen. Effect of N-substituents on performance of thiourea collectors by density functional theory calculations [J]. Transactions of Nonferrous Metals Society of China, 2010, 20(3): 695−701.

[18] YEKELER H, YEKELER M. Predicting the efficiencies of 2-mercaptobenzothiazole collectors used as chelating agents in flotation processes: a density-functional study [J]. J Mol Model, 2006, 12: 763−768.

[19] CHEN Ye, CHEN Jian-hua, GUO Jin. A DFT study on the effect of lattice impurities on the electronic structures and floatability of sphalerite [J]. Miner Eng, 2010, 23: 1120−1130.

[20] QIN Wen-qing, JIAO Fen, SUN Wei, WANG Xing-jie, LIU Bei, WANG Jun, ZENG Ke, WEI Qian, LIU Kai. Effects of sodium salt of N, N−dimethyldi−thiocarbamate on floatability of chalcopyrite, sphalerite, marmatite and its adsorption properties [J]. Colloids Surf A, 2013, 421: 181−192.

[21] HUNG A, MUSCAT J, YAROVSKY I, RUSSO S P. Density-functional theory studies of pyrite FeS_2 (100) and (110) surfaces [J]. Surf Sci, 2002, 513: 511−524.

[22] MUSCAT J, GALE J D. First principles studies of the surface of galena PbS [J]. Geochim Cosmochim Acta, 2003, 67: 799−805.

[23] MUSCAT J, HUNG A, RUSSO S, YAROVSKY I. First-principles studies of the structural and electronic properties of pyrite FeS_2 [J]. Phys Rev B: Condens Matter Mater Phys, 2002, 65: 054107.

[24] REICH M, BECKER U. First-principles calculations of the thermodynamic mixing properties of arsenic incorporation into pyrite and marcasite [J]. Chem Geol, 2006, 225: 278−290.

[25] RENOCK D, BECKER U. A first principles study of coupled substitution in galena [J]. Ore Geol Rev, 2011, 42: 71−83.

[26] STEELE H M, WRIGHT K, HILLIER I H. A quantum-mechanical study of the (110) surface of sphalerite (ZnS) and its interaction with Pb^{2+} species [J]. Phys Chem Miner, 2003, 30: 69−75.

[27] BLANCHARD M, ALFREDSSON M, BRODHOLT J, WRIGHT K, CATLOW C R A. Arsenic incorporation into FeS_2 pyrite and its influence on dissolution: A DFT study [J]. Geochim Cosmochim Acta, 2007, 71: 624−630.

[28] BLANCHARD M, WRIGHT K, GALE J D, CATLOW C R A. Adsorption of $As(OH)_3$ on the (001) surface of FeS_2 pyrite: A quantum-mechanical DFT study [J]. J Phys Chem C, 2007, 111: 11390−11396.

[29] von OERTZEN G U, SKINNER W M, NESBITT H W, PRATT A R, BUCKLEY A N. Cu adsorption on pyrite: Ab initio and spectroscopic studies [J]. Surf Sci, 2007, 601: 5794−5799.

[30] de OLIVEIRA C, de LIMA G F, de ABREU H A, DUARTE H A. Reconstruction of the chalcopyrite surfaces—A DFT study [J]. J Phys Chem C, 2012, 116: 6357−6366.

[31] de OLIVEIRA C, DUARTE H A. Disulphide and metal sulphide formation on the reconstructed (001) surface of chalcopyrite: A DFT study [J]. Appl Surf Sci, 2010, 257: 1319−1324.

[32] KLAUBER C. Fracture-induced reconstruction of a chalcopyrite ($CuFeS_2$) surface [J]. Surf Interface Anal, 2003, 35: 415−428.

[33] JONES M H. Some recent developments in the measurement and control of xanthate, perxanthate, sulphide, and redox potential in flotation [J]. Int J Miner Process, 1991, 33: 193−205.

[34] CHANDER S. A brief review of pulp potentials in sulfide flotation [J]. Int J Miner Process, 2003, 72: 141−150.

[35] TOLLEY W, KOTLYAR D, van WAGONER R. Fundamental electrochemical studies of sulfide mineral flotation [J]. Miner Eng, 1996, 9: 603−637.

[36] CHEN Jian-hua, CHEN Ye. A first-principle study of the effect of vacancy defects and impurities on the adsorption of O_2 on sphalerite surfaces [J]. Colloids Surf A, 2010, 363: 56−63.

[37] CHEN J, WANG L, CHEN Y, GUO J. A DFT study of the effect of natural impurities on the electronic structure of galena [J]. Int J Miner Process, 2011, 98: 132−136.

[38] de LIMA G F, de OLIVEIRA C U, de ABREU H A, DUARTE H L A. Water adsorption on the reconstructed (001) chalcopyrite surfaces [J]. J Phys Chem C, 2011, 115: 10709−10717.

[39] PERDEW J P, BURKE K, ERNZERHOF M. Generalized gradient approximation made simple [J]. Phys Rev Lett, 1996, 77: 3865−3868.

[40] KNIGHT K S, MARSHALL W G, ZOCHOWSKI S W. The low-temperature and high-prssure thermoelastic and structral properties of chalcopyrite, $CuFeS_2$ [J]. Can Mineral, 2011, 49: 1015−1034.

[41] SKINNER B J. Unit-cell edges of natural and synthetic sphalerites [J]. Am Mineral, 1961, 46: 1399−1411.

[42] HOPE G A, BUCKLEY F M, MUNCE C G, WOODS R. Gold enhanced spectroelectrochemical investigation of 2-mercaptobenzothiazole, isopropyl xanthate and butylethoxycarbonylthiourea adsorption on minerals [J]. Miner Eng, 2007, 20: 964−969.

[43] FLEMMIG B, SZARGAN R, REINHOLD J. Adsorption of mercaptobenzothiazole and similar molecules on cadmiumsulfide: A theoretical study [J]. J Phys Chem B, 2001,105: 5440−5449.

[44] FUKUI K. Theory of orientation and stereoselection [M]. Berlin: Springer, 1970.

[45] de LIMA G F, de OLIVEIRA C, de ABREU H A, DUARTE H A. Sulfuric and hydrochloric acid adsorption on the reconstructed sulfur terminated (001) chalcopyrite surface [J]. Int J Quantum Chem, 2012, 112: 3216−3222.

[46] MA H, CHEN S, LIU Z, SUN Y. Theoretical elucidation on the inhibition mechanism of pyridine–pyrazole compound: A Hartree fock study [J]. J Mol Struct, 2006, 774: 19−22.

巯基苯骈噻唑在黄铜矿和闪锌矿表面的吸附机理：第一性原理分析和光谱研究

焦 芬，覃文庆，刘瑞增，王兴杰

中南大学 资源加工与生物工程学院，长沙 410083

摘 要：通过红外光谱分析和密度泛函理论对 2-巯基苯骈噻唑(MBT)与黄铜矿和闪锌矿表面的作用机理进行研究。红外光谱分析结果表明，当药剂与矿物作用后，黄铜矿表面出现 MBT 的特征峰，包括 C═N，C═N—S 和 C—S 的伸缩振动峰，其表面出现吸附产物 CuMBT；但是，在闪锌矿表面未发现药剂 MBT 的特征峰。MBT 以硫酮分子形式存在时更稳定，N 原子和环外 S 原子易与金属发生反应，为反应活性位点。与闪锌矿(110)面相比，MBT 更容易吸附在黄铜矿(112)面，它是通过五元环外的 S 原子的 p 和 s 轨道与 Cu 原子的 d 轨道形成正配键，从而在黄铁矿表面发生吸附。在真空条件下，以硫酮分子形式存在的 MBT 很难自发地吸附在闪锌矿(110)面。

关键词：黄铜矿；闪锌矿；2-巯基苯骈噻唑；吸附机理；密度泛函理论

(Edited by Wei-ping CHEN)